計測自動制御学会東北支部 第202回研究集会 (2002.7.2)
資料番号 202-4

# Application of Reaction-less Motion to Teleoperation of a Flexible Base Dual-Arm Manipulator

○鷲野誠一郎*，Michael Shoemaker**，内山勝*

○Seiichiro Washino*, Michael Shoemaker**, Masaru Uchiyama*

*東北大学, **Virginia Polytechnic Institute and State University

*Tohoku University, **Virginia Polytechnic Institute and State University

**キーワード**： Flexible Structure mounted manipulator System, Reaction Null Space, reaction compensation

**連絡先**： 〒980-8579 仙台市青葉区荒巻字青葉01 東北大学 大学院工学研究科 航空宇宙工学専攻
宇宙航空制御学講座宇宙機械学分野(内山研究室)
鷲野誠一郎，Tel.: (022)217-6973，Fax.: (022)217-6971，E-mail: washino@space.mech.tohoku.ac.jp

## 1. Introduction

A robotic manipulator designed for space applications is strongly desired to be lightweight and capable of fast movement because of limitation of launch vehicle payload weight, restrictive launch costs, and limited mission duration. In such situations, a long-reach manipulator system, which consists of a series of small manipulators attached to the end of a long manipulator, able to keep a large workspace and also do precise work, is proposed. We can regard the long manipulator as a flexible arm because of its low rigidity. Though its accuracy of work isn't assured, it can keep a large workspace because it has a large reachable range. On the other hand, small manipulators attached to the end of the long manipulator don't have a large reachable range, but they can do more precise and accurate work due to their high rigidity. Some notable examples are the Special Purpose Dexterous Manipulator (SPDM) mounted on the Space Station Remote Manipulator System (SSRMS)[1], and the Japanese Experimental Module Small Fine Arm attached to the Remote Manipulator System (JEMRMS)[2].

When we control this kind of system, problems associated with flexibility of the long-reach manipulator emerge. Namely, when the rigid manipulators move after being issued control commands, a reaction force and moment are transferred to the base of the long flexible arm and subsequent vibration occurs. This vibration may bring performance penalties, so we must solve this problem of vibration to operate it practically.

During practical operation, it is realistic that the long-reach manipulator is first used to decide the general position of the end-effector, after which only the rigid manipulators work for the remainder of the task. In this case, the long-reach manipulator

acts on a flexible base on which the rigid manipulators are mounted. Therefore, when we focus our attention on the rigid manipulators, we can regard this vibration problem as similar to that of a Flexible Structure mounted manipulator System (FSMS). Many studies on controlling FSMS have been done.

The experimental system designed in this lab consists of a dual-arm manipulator, with each arm having two links and two joints and capable of movement in a two-dimensional plane, mounted on the end of a one link flexible arm. This system, named TREP, was previously used in both single and dual arm configurations to study reaction-less motion and vibration suppression control with Reaction Null Space[3, 4, 5, 7, 8]. Especially in the case of a dual-arm configuration, reaction compensation control was studied[5, 8]. Finally, when applying these principles to the practical work of transporting an object, the method using reaction-less motion and vibration suppression control was considered[6].

In this study, we consider the case where precise work is accomplished by a human operator through teleoperation. Specifically, one arm of the flexible structure mounted dual manipulator system is teleoperated freely, with reaction compensation control provided by the other arm automatically.

# 2. TREP Experimental System

## 2.1 TREP Experimental Robot

An illustration of TREP is shown in Figure 1. TREP consists of a dual-arm manipulator, with each arm having two links and two joints and capable of movement in a two-dimensional plane, mounted vertically on the end of a one link flexible arm.

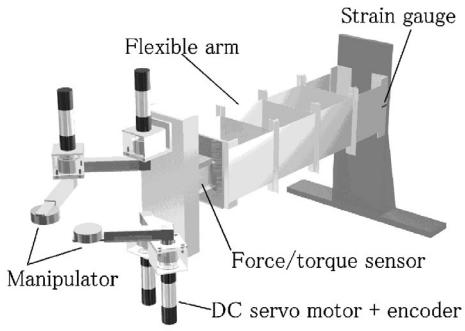


Fig. 1 Illustration of TREP

A DC servomotor powers each joint on the rigid manipulators. A strain gauge attached to the root part of the flexible arm is used to measure the deflection of the end of the flexible arm. A three axis force/torque sensor is attached to the end of the flexible arm to sense the reaction force and moment caused by the movement of the rigid manipulators.

## 2.2 Control System of TREP

The control system of TREP is shown in Figure 2. The main computer used to control TREP is a 32 [bit] Dell Dimension 2100 PC (CPU: Celeron 800 [MHz]) which runs the real-time operating system VxWorks. The joint angles of the motors of the rigid manipulators are sensed by the encoders. The pulses from the encoders are sent to the motor driver, which in turn uses the pulses both to feedback the angular velocity and to send the value of the joint angle to the main computer. The signals from the strain gauge on the force/torque sensor and on the root part of the flexible arm are sent to the main computer through the strain amplifier and the A/D converter. The main computer calculates the values of each joint angle, and sends the values back to the motor driver through the D/A converter.

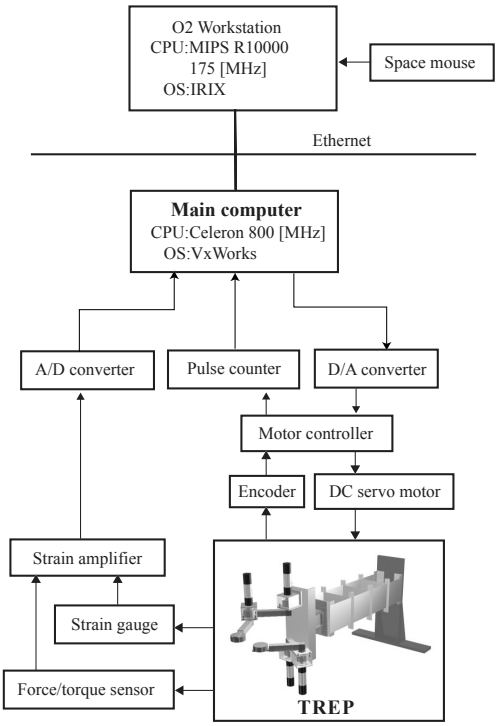


Fig. 2 Control system of TREP

For us to send the command to one arm of TREP by teleoperation, the command first needs to be received by an input device and displayed to the operator in visual form. For this purpose, a Silicon Graphics O2 workstation (CPU: MIPSR10000, 175 [MHz]) running IRIX is used because of its powerful graphics rendering capability. The object-oriented graphical toolkit Open Inventor is used as the application programming interface. Motion commands are input via a six DOF pointer called Space Mouse manufactured by LogiTech. The refresh rate of the display and the sampling rate at which input values are collected from Space Mouse are both once every 20 [ms]. At the same time, the reference joint angle and the angular velocity of the upper arm are calculated, and then sent to the main computer through socket connection.

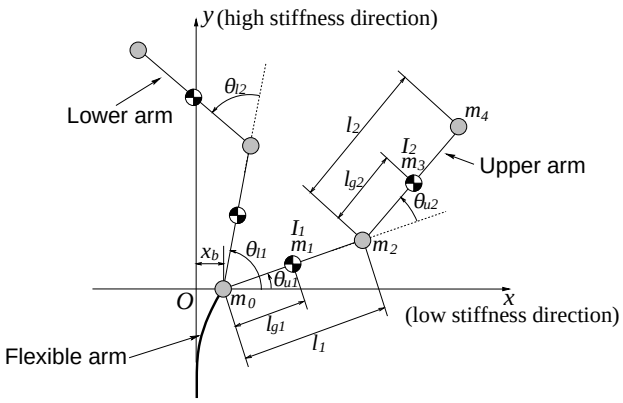


Fig. 3 Model of TREP

# 3. Dynamics Model of TREP and Equation of Reaction Compensation Control

## 3.1 Dynamics Model of TREP

The dynamics of TREP can be considered as an FSMS that consists of a dual-arm rigid manipulator, with each arm having two links and two joints and capable of movement in a two-dimensional plane, mounted vertically on the end of a one link flexible arm (Figure 3). Since both rigid manipulators have the same layout and are attached vertically atop one another on the base, we refer to them as the upper arm and lower arm. The origin point of the frame of this system is defined as the point where the end of the flexible arm would be with zero vibration. We define the $x$-axis and $y$-axis of the coordinate system as the low stiffness direction and high stiffness direction of the flexible arm, respectively. Because of the feature of a parallel board spring, we can assume that the orientation of the frame remains constant regardless of deflection of the flexible arm. The joint angles $\theta_{u1}$, $\theta_{u2}$, $\theta_{l1}$, $\theta_{l2}$ are defined as shown in Figure 3.

### 3.2 Equation of Reaction Compensation Control

The equation of motion of the base can be expressed as follows in (1). Here, base deflection in the $x$ direction is $x_b$, and base deflection in the $y$ direction is taken to be zero.

$$\boldsymbol{H}_{bmu}(\boldsymbol{\theta}_u)\ddot{\boldsymbol{\theta}}_u + \boldsymbol{H}_{bml}(\boldsymbol{\theta}_l)\ddot{\boldsymbol{\theta}}_l + C_b(\dot{\boldsymbol{\theta}}_u, \boldsymbol{\theta}_u, \dot{\boldsymbol{\theta}}_l, \boldsymbol{\theta}_l) + H_b\ddot{x}_b + k_b x_b = 0 \quad (1)$$

where,

| | | |
|---|---|---|
| $\boldsymbol{\theta}_u \in \boldsymbol{R}^2$ | : | joint angle of the upper arm |
| $\boldsymbol{\theta}_l \in \boldsymbol{R}^2$ | : | joint angle of the lower arm |
| $\boldsymbol{H}_{bmu}(\boldsymbol{\theta}_u) \in \boldsymbol{R}^{1\times 2}$ | : | inertia coupling matrix of the upper arm |
| $\boldsymbol{H}_{bml}(\boldsymbol{\theta}_l) \in \boldsymbol{R}^{1\times 2}$ | : | inertia coupling matrix of the lower arm |
| $H_b$ | : | elastic base inertia coefficient |
| $C_b(\dot{\boldsymbol{\theta}}_u, \boldsymbol{\theta}_u, \dot{\boldsymbol{\theta}}_l, \boldsymbol{\theta}_l)$ | : | non-linear Coriolis and centrifugal terms |
| $k_b$ | : | elastic base stiffness coefficient |
| $x_b$ | : | elastic base $x$ direction deflection |

Considering that $\boldsymbol{C}_b$ is equivalent to $\dot{\boldsymbol{H}}_{bmu}\dot{\boldsymbol{\theta}}_u + \dot{\boldsymbol{H}}_{bml}\dot{\boldsymbol{\theta}}_l$, we can divide (1) into $\boldsymbol{\theta}_u$ , $\boldsymbol{\theta}_l$ term and $x_b$ term.

$$\boldsymbol{H}_{bmu}(\boldsymbol{\theta}_u)\ddot{\boldsymbol{\theta}}_u + \boldsymbol{H}_{bml}(\boldsymbol{\theta}_l)\ddot{\boldsymbol{\theta}}_l + \dot{\boldsymbol{H}}_{bmu}\dot{\boldsymbol{\theta}}_u + \dot{\boldsymbol{H}}_{bml}\dot{\boldsymbol{\theta}}_l = -H_b\ddot{x}_b - k_b x_b \quad (2)$$

From this, we can see that the left side of equation (2) affects the base deflection $x_b$, so these terms can be regarded as the reaction force acting on the base. Calling this reaction force $\mathcal{F}$, the equation is rewritten as,

$$\mathcal{F} = \boldsymbol{H}_{bmu}(\boldsymbol{\theta}_u)\ddot{\boldsymbol{\theta}}_u + \boldsymbol{H}_{bml}(\boldsymbol{\theta}_l)\ddot{\boldsymbol{\theta}}_l + \dot{\boldsymbol{H}}_{bmu}\dot{\boldsymbol{\theta}}_u + \dot{\boldsymbol{H}}_{bml}\dot{\boldsymbol{\theta}}_l \quad (3)$$

Thus, when $\mathcal{F}$ is zero, no reaction force is acting on the base. If we integrate (3) with respect to time, the result is,

$$\mathcal{L} = \boldsymbol{H}_{bmu}\dot{\boldsymbol{\theta}}_u + \boldsymbol{H}_{bml}\dot{\boldsymbol{\theta}}_l = \text{const} \quad (4)$$

If we make the assumption that there is no initial base movement, $\mathcal{L}$ is zero. Now, if we solve (4) for $\dot{\boldsymbol{\theta}}_l$, considering that the lower arm compensates the reaction force of the upper arm, the equation is expressed as,

$$\dot{\boldsymbol{\theta}}_l = -\boldsymbol{H}^+_{bml}\boldsymbol{H}_{bmu}\dot{\boldsymbol{\theta}}_u \quad (5)$$

where $\boldsymbol{H}^+_{bml}$ denotes the right pseudo inverse of $\boldsymbol{H}_{bml}$. This solution expresses the angular velocity of the lower arm which compensates the $x$ component of the reaction force caused by the upper arm of TREP.

## 4. Inverse Kinematics and Jacobian of TREP

When we calculated the part of the command dealing with the teleoperation of the upper arm, we used the inverse kinematics and the inverse Jacobian matrix. Before explaining the method of control, we will outline these equations briefly.

### 4.1 Inverse Kinematics of TREP

The equation of kinematics of the upper arm can be easily derived from Figure 3, which is written as follows,

$$\begin{aligned} \boldsymbol{r}_{au} &= \begin{bmatrix} x_{au} \\ y_{au} \end{bmatrix} \\ &= \begin{bmatrix} l_1\cos\theta_{u1} + l_2\cos(\theta_{u1}+\theta_{u2}) \\ l_1\sin\theta_{u1} + l_2\sin(\theta_{u1}+\theta_{u2}) \end{bmatrix} \end{aligned} \quad (6)$$

where $\boldsymbol{r}_{au}$ is the position of the end point of the upper arm, keeping in mind that the reference frame of $\boldsymbol{r}_{au}$ remains fixed on the base. Applying the

cosine theorem to (6), the equation of inverse kinematics is written as,

$$\begin{aligned}\theta_{u1} &= \arctan\left(\frac{y_{au}}{x_{au}}\right) \\ &\quad \mp \arctan\left(\frac{\kappa}{x_{au}^2+y_{au}^2+l_1^2-l_2^2}\right) \\ \theta_{u2} &= \pm \arctan\left(\frac{\kappa}{x_{au}^2+y_{au}^2-l_1^2-l_2^2}\right)\end{aligned}$$

where,

$$\kappa = \sqrt{(x_{au}^2+y_{au}^2+l_1^2+l_2^2)^2-2((x_{au}^2+y_{au}^2)^2+l_1^4+l_2^4)}$$

As can been seen above, $\kappa$ is only defined where, $0 < x_{au}^2+y_{au}^2 \leqq l_1^2+l_2^2$. Now, we must choose from the above two equations the form of the inverse kinematics equation we want to use to express our experimental configuration. The equations used in the experiment are,

$$\begin{aligned}\theta_{u1} &= \arctan\left(\frac{y_{au}}{x_{au}}\right) \\ &\quad + \arctan\left(\frac{\kappa}{x_{au}^2+y_{au}^2+l_1^2-l_2^2}\right) \quad (7) \\ \theta_{u2} &= -\arctan\left(\frac{\kappa}{x_{au}^2+y_{au}^2-l_1^2-l_2^2}\right) \quad (8)\end{aligned}$$

Expressed in this manner, negative values of $\theta_{u2}$ decide the posture of the arm. With these equations, there is a one to one correspondence of the end point position of the upper arm and the joint angles, and we can calculate the joint angles from the position. It can also be seen that the singular point of this equation is the origin, meaning when the upper arm is positioned so that the end point is located at the origin, the solution is undefined, and the one joint angle can't be decided by the one position.

## 4.2 Jacobian of TREP

As explained previously, $\boldsymbol{r}_{au}$ is the position of the end point of the upper arm, where the reference frame of $\boldsymbol{r}_{au}$ remains fixed on the base. If (6) is differentiated with respect to time, the equation is written as,

$$\dot{\boldsymbol{r}}_{au} = \boldsymbol{J}_u \dot{\boldsymbol{\theta}}_u \quad (9)$$

where,

$$\begin{aligned}\dot{\boldsymbol{r}}_{au} &= \begin{bmatrix} \dot{x}_{au} & \dot{y}_{au} \end{bmatrix}^T \\ \dot{\boldsymbol{\theta}}_u &= \begin{bmatrix} \dot{\theta}_{u1} & \dot{\theta}_{u2} \end{bmatrix}^T\end{aligned}$$

Then, the Jacobian of the upper arm is written as,

$$\boldsymbol{J}_u = \begin{bmatrix} -l_1S_{u1}-l_2S_{u12} & -l_2S_{u12} \\ l_1C_{u1}+l_2C_{u12} & l_2C_{u12} \end{bmatrix} \quad (10)$$

where,

$$\begin{aligned}S_{u1} &= \sin\theta_{u1} \\ S_{u2} &= \sin\theta_{u2} \\ S_{u12} &= \sin(\theta_{u1}+\theta_{u2}) \\ C_{u1} &= \cos\theta_{u1} \\ C_{u2} &= \cos\theta_{u2} \\ C_{u12} &= \cos(\theta_{u1}+\theta_{u2})\end{aligned}$$

If we multiply both sides of (9) by $\boldsymbol{J}_u^{-1}$, the equation can be rewritten as,

$$\dot{\boldsymbol{\theta}}_u = \boldsymbol{J}_u^{-1}\dot{\boldsymbol{r}}_{au} \quad (11)$$

where,

$$\boldsymbol{J}_u^{-1} = \frac{1}{l_1l_2S_{u2}}\begin{bmatrix} l_2C_{u12} & l_2S_{u12} \\ -l_1C_{u1}-l_2C_{u12} & -l_1S_{u1}-l_2S_{u12} \end{bmatrix} \quad (12)$$

With this equation, there is a one to one correspondence of the upper arm end point velocity to the joint angular velocity, and thus the joint angular velocity can be calculated from the end point velocity. It can also be realized that the singular positions are points such that,

$$\theta_{u2} = n\pi \qquad (n = 0, 1, 2, \ldots)$$

These positions correspond to the manipulator either being fully extended or folded in on itself. As the manipulator approaches these conditions, the closer to infinity the value of the joint angular velocity becomes.

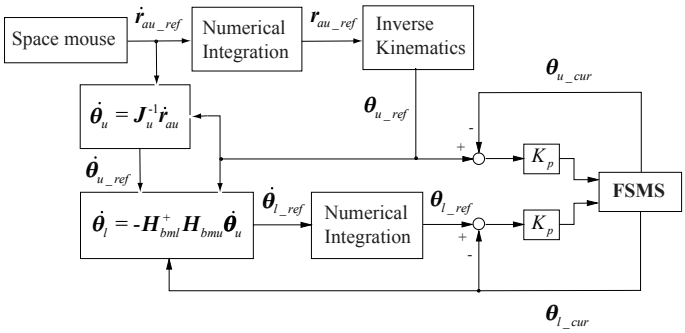


Fig. 4 Block diagram of the control

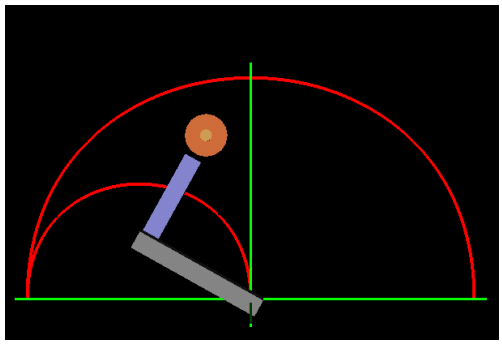

Fig. 5 CG display of upper arm of TREP

# 5. Experiment of Reaction Compensation Control by Teleoperation

## 5.1 Method of Control and Block Diagram

In this experiment, the upper arm is moved using the velocity command generated by Space Mouse, and the lower arm is moved using (5). The block diagram for this control is shown in Figure 4, where $K_p$ expresses a proportional gain.

The following calculations are done in the O2 workstation. First, the reference velocity of the upper arm $\dot{\boldsymbol{r}}_{au\_ref}$ is taken from Space Mouse and numerically integrated with respect to time to yield the reference position of the upper arm, $\boldsymbol{r}_{au\_ref}$, which is used for the following: the reference joint angle of the upper arm $\boldsymbol{\theta}_{u\_ref}$ is calculated using the inverse kinematics equations, and the reference joint angular velocity of the upper arm $\dot{\boldsymbol{\theta}}_{u\_ref}$ is calculated with (11) using both the reference velocity of the upper arm $\dot{\boldsymbol{r}}_{au\_ref}$ and the reference joint angle of the upper arm $\boldsymbol{\theta}_{u\_ref}$.

The next part of the control scheme is calculated in the main computer. After the reference joint angle of the upper arm $\boldsymbol{\theta}_{u\_ref}$ is calculated, it is used according to equation (5) with the reference joint angular velocity of the upper arm $\dot{\boldsymbol{\theta}}_{u\_ref}$ and the current joint angle of the lower arm $\boldsymbol{\theta}_{l\_cur}$ to calculate the reference joint angular velocity of the lower arm $\dot{\boldsymbol{\theta}}_{l\_ref}$. This angular velocity is then numerically integrated with respect to time to yield the reference joint angle of the lower arm $\boldsymbol{\theta}_{l\_ref}$. After this, the upper and lower arm move according to their respective reference angles with proportional control.

By using the above described control method, it is possible for the operator to control the upper arm at any desired reference velocity using Space Mouse, causing the lower arm to compensate the reaction force.

## 5.2 Visual Display of Command Input

When movement commands are issued to TREP via the Space Mouse, the operator is working from a location removed from that of the actual TREP unit. Therefore, the O2 workstation is used to draw a CG display of the upper arm of TREP as a visual cue to the operator. The CG display is shown in Figure 5.

The teleoperating system of TREP is shown in Figure 6. The refresh rate of the display and the sampling rate at which input values are collected

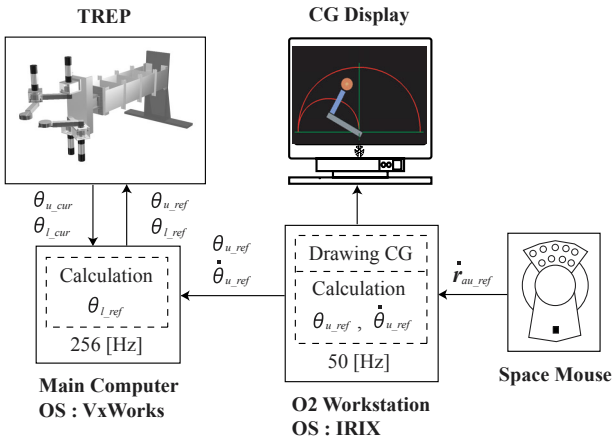


Fig. 6 Teleoperating system diagram of TREP

from Space Mouse are both once every 20 [ms], in other words, at a frequency of 50 [Hz]. After that, the reference joint angle and the angular velocity of the upper arm are calculated as described previously, and then sent to the main computer through socket connection. The reference joint angle is also used to render the upper arm on the display, making it possible for us to show the reference velocity to the operator at a rapid rate.

The two half circles on the display represent the boundaries in which the upper arm can move. We determined this range as,

$$x^2 + y^2 \leqq 360, \ and \ (x+10)^2 + y^2 \geqq 95, \ and \ y \geqq 0$$

This is intentionally set slightly smaller than the actual mechanical range of the upper arm so as not to let the upper arm approach the singular points that we have explained before. We didn't consider the singular point of the equations of the inverse kinematics because we assumed that there is little chance that the operator would generate the commands necessary to approach the specific singular point. However, the singular points of (11), especially the case where the arm is fully extended, can easily be caused by the operator. Hence, the upper arm mustn't be allowed to approach this limit too closely, because as the arm approaches its fully extended posture, the value of the reference joint angular velocity approaches infinity. Thus the reason for the boundaries as shown on the CG display.

## 5.3 Experimental Conditions

In the first experiment, the upper arm is moved as described previously by the velocity command created by Space Mouse. The experimental conditions are as follows,

- Initial position
  Upper arm : $\boldsymbol{\theta}_u = \begin{bmatrix} 180^\circ & -90^\circ \end{bmatrix}^T$
  Lower arm : $\boldsymbol{\theta}_l = \begin{bmatrix} 0^\circ & 90^\circ \end{bmatrix}^T$
- Time duration = 5.0 [s]
- Sampling frequency = 256 [Hz]
- Proportional gain $K_p = 100$ [$s^{-1}$]
- Lowpass filter cutoff = 2.0 [Hz]

Despite the high sampling frequency of 256 [Hz], the movement commands generated by the operator are collected and sent to the main computer at a rate of only once per 20 [ms]. This fact caused movement commands that were too jagged in appearance, so our solution was to use a single-order interpolation in the main computer to approximate position values.

As a comparative experiment, we repeated the first experiment but with no reaction compensation control supplied by the lower arm. The same upper arm movement commands from the first experiment are reused so that the only difference between the two trials is the presence of lower arm movement.

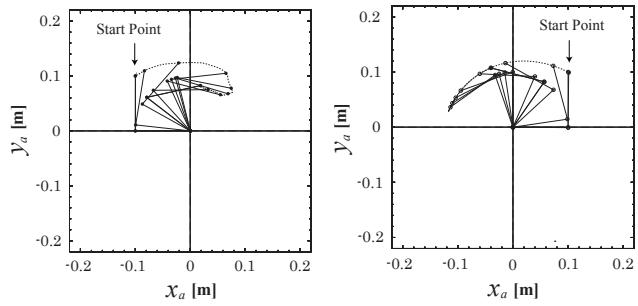


(a) Upper arm (b) Lower arm

Fig. 7 The movement of the both arms

## 5.4 Experimental Results

The movement of both arms in the experiment with reaction compensation control are shown in Figure 7. Plots of the data collected from both experiments are shown in Figure 8. Parts (a) and (b) of the figure show the upper arm joint angles, $\theta_{u1}$ and $\theta_{u2}$, respectively. Parts (c) and (d) show the lower arm joint angles, $\theta_{l1}$ and $\theta_{l2}$, respectively. Part (e) shows the $x$ and $y$ components of the reaction force, $F_x$ and $F_y$, caused by manipulator movement. Finally, part (f) shows the deflection of the flexible arm. The results from the experiment with no reaction compensation control are likewise shown in Figure 9.

## 5.5 Interpretation of Results

First, we will consider the results in terms of the performance of the experimental reaction compensation control of TREP. In the case where reaction compensation control is used, the force in the low rigidity direction, $F_x$, remains low, and the maximum deflection of the base does not exceed 1 [mm]. Conversely, in the case where there is no reaction compensation, the same upper arm movement causes greater $F_x$ and a greater maximum deflection of almost 3 [mm]. This is most pronounced at around time 2.0 [s], when the upper arm velocity changes direction along the $x$-axis rapidly as seen in part (a) of Figure 9. It follows intuitively that an acceleration of the manipulator in the low-stiffness direction in the absence of any reaction compensation will cause a force and a subsequent vibration of the base. Therefore, the fact that there is little base deflection in the presence of high acceleration of the manipulator as seen in the first experiment shows that the reaction compensation control provided by (5) is effective. It should be noted, however, that slight vibration of the base can still be seen even when reaction compensation is used. The cause of this vibration may be the big and sudden change of the reference joint angular velocity of the upper arm when its value is also big. The command created by teleoperation may tend to be like this. When the value of the reference joint angular velocity is big, the reference joint angle calculated as the command is rough, and more when the value of the reference joint angular velocity changes suddenly, the accuracy of realizing (5) may be going down. In this experiment, we can see the sudden change of the reference joint angular velocity at around time from 1.5 to 2.0 [s] in both joint of the upper arm, and this seems to make the vibration.

Second, we will consider the results in terms of the experimental teleoperation of TREP. In our experiments, the operator relied on a CG representation of the movement commands to control TREP. We found that it was effective to show the movable range in the display, including the consideration of the singular points of the upper arm, as a way to let the operator choose appropriate commands. While still developing the system, we found that it was a very difficult task to control the upper arm by simply looking at TREP without the

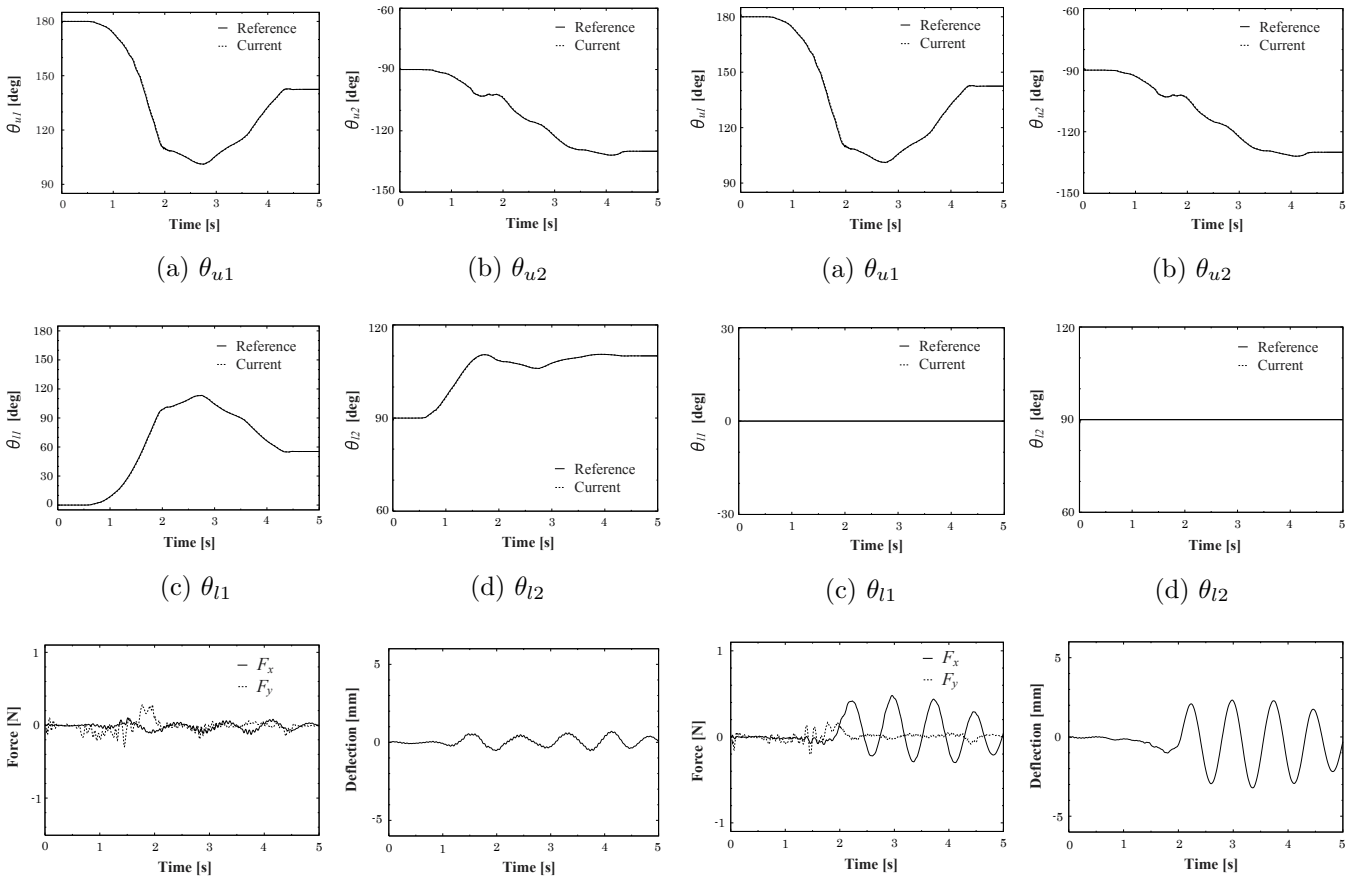


(a) $\theta_{u1}$ (b) $\theta_{u2}$

(c) $\theta_{l1}$ (d) $\theta_{l2}$

(e) Reaction force (f) Base deflection ($x$)

Fig. 8 Results of experiment with compensation




(a) $\theta_{u1}$ (b) $\theta_{u2}$

(c) $\theta_{l1}$ (d) $\theta_{l2}$

(e) Reaction force (f) Base deflection ($x$)

Fig. 9 Results of experiment with no compensation

CG display. It was especially easy to inadvertently approach the outer boundary, represented by the large half-circle, making manipulation tasks very difficult.

There are additional factors that should be considered when implementing a CG display as we did. In cases where a robot manipulator has a relatively simple configuration of links and joints–as does TREP, with two links and two joints per arm–it is somewhat easy for the operator to imagine the singular points and the limits on movable range of the manipulator being controlled. But in cases where the manipulator has a complicated structure, it might be too difficult for the operator to do this mentally while performing teleoperation tasks. This is where a CG display of the movable range of the manipulator becomes a necessity. Also, in the CG display used in our experiments, the movable range was shown for the upper arm, but no consideration was given to displaying the movable range of the lower arm, which compensated the reaction force. As a result, even if the upper arm was operated within its limits, sometimes the lower arm would move in an undesirable fashion, causing more vibration than it was supposed to compensate. This highlights the additional need, in cases similar to our experimental system, for a display that incorporates the movable ranges of both the directly and indirectly controlled arms teleoperated manually by the human operator.

# 6. Conclusion

We have considered the case where precise work is accomplished by a human operator through teleoperation. With the experimental system TREP, we teleoperated one arm of the flexible structure mounted dual manipulator system freely with reaction compensation control provided by the other arm automatically.

From the results, in terms of the performance of the experimental reaction compensation control of TREP, we can recognize the method of control is effective. But, because of the inability of the system to realize control equation (5) under certain conditions, small vibration occured even with the lower arm compensating. When we consider the results in terms of the experimental teleoperation, in cases similar to our experimental system, we should need a display that incorporates the movable ranges of both the directly and indirectly controlled arms teleoperated manually by the human operator.

# References


1) C. Vallancourt, C. M. Gosselin: Compensating for the structural flexibility of SSRMS with the SPDM, 2nd Workshop on Robotics in Space, Canadian Space Agency, Montreal, Canada, (1994)
2) F. Kuwao, et al.: Dynamic Performance of Japanese Experiment Module Remote Manipulator System, Proceedings of the International Symposium on Artificial Intelligence, Robotics and Automation in Space, Tokyo, Japan, 205/210 (1997)
3) D.N. Nenchev, K. Yoshida, P. Vichitkulsawat, A. Konno, M. Uchiyama: Experiments on Reaction Null-Space Based Decoupled Control of a Flexible Structure Mounted Manipulator System, Proceedings of the 1997 IEEE International Conference on Robotics and Automation, Albuquerque, New Mexico, USA, 2528/2534 (1997)
4) 吉田和哉，D．ネンチェフ，郷緒昭夫，猿橋直哉，内山勝: 柔軟ベースロボットの反動制御，日本機械学会 ロボティクス・メカトロニクス講演会'97 講演論文集，**97**-22，197/198，(1997)
5) A. Gouo, D. N. Nenchev, K. Yoshida, M. Uchiyama: Dual-Arm Long-Reach Manipulators: Noncontact Motion Control Strategies, Proceeding of the 1998 IEEE/RSJ International Conference on Intelligent Robots and Systems, Victoria, B.C., Canada, 449/454 (1998)
6) 谷口優，Dragomir N. Nenchev, 吉田和哉，内山勝: 柔軟ベース上マニピュレータの作業計画と制御，日本機械学会 ロボティクス・メカトロニクス講演会'99 講演論文集，**99**-9，1A1-06-021(1)/(2)，(1999)
7) Dragomir N. Nenchev, Kazuya Yoshida, Prasert Vichitkulsawat, and Masaru Uchiyama: Reaction Null-Space Control of Flexible Structure Mounted Manipulator Systems, IEEE TRANSACTIONS ON ROBOTICS AND AUTOMATION, **15**-6, 1011/1023 (1999)
8) A. Gouo, Dragomir N. Nenchev, Kazuya Yoshida and Masaru Uchiyama: Motion control of dual-arm long-reach manipulators, Advanced Robotics, **13**-6, 617/631 (2000)